Published in final edited form as:
JACC Cardiovasc Interv. 2011 December ; 4(12): 1318–1325. doi:10.1016/j.jcin.2011.07.017.

Direct Percutaneous Left Ventricular Access and Port Closure:

Pre-Clinical Feasibility

Israel M. Barbash, MD[*], **Christina E. Saikus, PhD**[*], **Anthony Z. Faranesh, PhD**[*], **Kanishka Ratnayaka, MD**[*,‡], **Ozgur Kocaturk, PhD**[*], **Marcus Y. Chen, MD**[*], **Jamie A. Bell, BS**[*], **Renu Virmani, MD**[†], **William H. Schenke, BS**[*], **Michael S. Hansen, PhD**[*], **Michael C. Slack, MD**[‡], and **Robert J. Lederman, MD**[*]

[*]Cardiovascular and Pulmonary Branch, Division of Intramural Research, the National Heart Lung and Blood Institute, National Institutes of Health, Bethesda, Maryland [†]CVPath, Gaithersburg, Maryland [‡]Children's National Medical Center, Washington, DC

Abstract

Objectives—This study sought to evaluate feasibility of nonsurgical transthoracic catheter-based left ventricular (LV) access and closure.

Background—Implanting large devices, such as mitral or aortic valve prostheses, into the heart requires surgical exposure and repair. Reliable percutaneous direct transthoracic LV access and closure would allow new nonsurgical therapeutic procedures.

Methods—Percutaneous direct LV access was performed in 19 swine using real-time magnetic resonance imaging (MRI) and an "active" MRI needle antenna to deliver an 18-F introducer sheath. The LV access ports were closed percutaneously using a commercial ventricular septal defect occluder and an "active" MRI delivery cable for enhanced visibility. We used "permissive pericardial tamponade" (temporary fluid instillation to separate the 2 pericardial layers) to avoid pericardial entrapment by the epicardial disk. Techniques were developed in 8 animals, and 11 more were followed up to 3 months by MRI and histopathology.

Results—Imaging guidance allowed 18-F sheath access and closure with appropriate positioning of the occluder inside the transmyocardial tunnel. Of the survival cohort, immediate hemostasis was achieved in 8 of 11 patients. Failure modes included pericardial entrapment by the epicardial occluder disk (n = 2) and a true-apex entry site that prevented hemostatic apposition of the endocardial disk (n = 1). Reactive pericardial effusion (192 ± 118 ml) accumulated 5 ± 1 days after the procedure, requiring 1-time drainage. At 3 months, LV function was preserved, and the device was endothelialized.

Conclusions—Direct percutaneous LV access and closure is feasible using real-time MRI. A commercial occluder achieved hemostasis without evident deleterious effects on the LV. Having established the concept, further clinical development of this approach appears realistic.

Reprint requests and correspondence: Dr. Robert J. Lederman, National Institutes of Health, 10 Center Drive, Building 10, Room 2c713, Bethesda, Maryland 20892-1538. lederman@nih.gov.

Drs. Barbash and Saikus contributed equally to this paper.

All other authors have reported that they have no relationships relevant to the contents of this paper to disclose.

Keywords

hybrid surgical procedures; interventional magnetic resonance imaging; periventricular; transcatheter aortic valve replacement

Safe and reliable direct percutaneous access and closure of left ventricular (LV) access ports would enable a range of cardiac and vascular interventions currently feasible only with surgery. These might include percutaneous transapical aortic valve replacement (1–3), mitral valve repair and replacement (4,5), and retrograde aortic root endograft procedures (6).

Direct LV access risks injury to critical structures, including the ventricular septum (7) or coronary arteries (8) and requires immediate recognition of procedural complications, including pericardial tamponade or hemothorax (9). Real-time magnetic resonance imaging (MRI) depicts blood and cardiac soft tissue in a larger thoracic context, making it an attractive tool to guide interventional procedures (10,11).

We hypothesized that real-time MRI could guide large percutaneous LV access port placement in a closed-chest, beating heart procedure and, thereafter, closure of the myocardial access port without surgery.

Methods

Animals

Animal procedures were conducted according to contemporary National Institutes of Health guidelines, in 19 naive Yorkshire swine (43 ± 9 kg). Eight animals were used for technique development and 11 were kept alive and assigned to up to 3 months of follow-up. Animals were pre-treated with aspirin and amiodarone. Anesthesia was maintained with inhaled isoflurane and mechanical ventilation.

Before LV access, a subxiphoid pericardial drainage catheter (8.3-F, Boston Scientific, Natick, Massachusetts) was placed under x-ray fluoroscopy, and the femoral artery and vein were accessed percutaneously for monitoring (12).

Active interventional equipment

For cardiac puncture, an 18-gauge, MRI-compatible (nickel-titanium-chromium) needle was customized for “active profiling” (visibility along its entire length during MRI) by integrating a loop coil along the needle shaft. Characteristic spacing between needle marker coils assisted in distinguishing the needle shaft from the tip.

The LV puncture site was closed with a commercial 6-mm muscular ventricular septal defect (VSD) occluder (AGA Medical, Plymouth, Minnesota). Unmodified devices were used in initial technique development, and modified devices (replacing the microscrew stainless steel with titanium to minimize MRI artifacts) (Fig. 1) were implanted in the survival cohort.

A custom delivery cable for the VSD occluder was developed to enhance visibility and reduce MRI artifacts. It incorporated a loopless antenna and had its steel mating microscrew replaced with titanium. The antenna was tuned so that MRI signal was maximal when the attached occluder achieved the fully deployed state before release.

Active devices were connected to a separate MRI receiver channel, and a device-related signal was independently colored and overlaid on real-time images (13).

Percutaneous LV access

All procedures were performed under real-time MRI guidance, with multiple continuously updated slices (Fig. 2).

An apical puncture trajectory was selected in consideration of the following: 1) avoiding bony structures of the chest; 2) the shortest distance to the heart; 3) avoiding coronary arteries; 4) the desired LV needle entry target, whether apical or para-apical; 5) avoiding injury to intracavitary structures (papillary muscles and interventricular septum); and 6) further intracavitary trajectories toward aortic or mitral valve structures.

An “active” 18-gauge needle was advanced from a selected thoracic skin location and, based on the position of the needle microcoils, the final trajectory was planned, and the needle was advanced into the LV cavity. An 18-F sheath (Cook Medical, Bloomington, Indiana) was delivered over a 0.035-inch Nitrex guidewire (ev3, Plymouth, Minnesota). A second, backup nitinol guidewire was also positioned alongside the sheath.

Heparin was administered to achieve an activated clotting time ≥250 s immediately following sheath placement and during and after closure to “stress” the test of immediate hemostasis.

Percutaneous LV closure

Percutaneous LV closure was performed with the muscular VSD occluder, under real-time MRI guidance. In an effort to avoid pericardial entrapment by the occluder, saline was instilled into the pericardial space guided by real-time MRI immediately before device deployment temporarily to separate the 2 pericardial layers (“permissive pericardial tamponade”) (12). A 6-mm VSD occluder was deployed using standard techniques (14). Finally, the instilled pericardial fluid was aspirated.

Magnetic resonance imaging

Interventions were performed in a 1.5-T MRI scanner (Espree, Siemens, Erlangen, Germany) using standard surface body receive coils. The wide (70-cm) bore allows operator access to the chest of large animals that we predict would translate to patients. MRI was used to guide all interventional procedures and for geometry and function measurements of the LV, pleural and pericardial fluid assessment, and myocardial scar.

For interventional procedures, we used real-time balanced steady state free precession (repetition time/echo time: 3.67/1.23 ms; flip angle: 45°; field of view: 340 × 255 mm; matrix: 192 × 144 pixels; slice thickness: 6 mm; and bandwidth: 789 Hz/pixel; parallel imaging and undersampling provided 3 to 5 frames/s). Images were reconstructed and displayed to the operator on a separate real-time workstation (13).

Cardiac computed tomography (CT) angiography roadmaps coregistered with real-time MRI

To avoid coronary artery injury, we used a cardiac CT angiography-derived 3-dimensional road map of the coronary tree overlaid on the real-time MRI.

Electrocardiogram-gated cardiac CT angiography was performed in a nonspiral mode on a 320-slice CT scanner (Aquilion ONE, Toshiba Medical Systems, Tokyo, Japan) using 16-cm detector coverage, 100-kV tube voltage, 550-mA tube current, and 350-ms gantry rotation time. The CT surface model and MRIs were manually registered to each other using anatomic landmarks, such as the aortic arch and coronary ostia (3D Slicer, Slicer.org, Brigham and Women’s Hospital, Boston, Massachusetts). After registration to the MRI

volume, the coronary volume was imported into the real-time workstation (IFE, Siemens Corporate Research, Princeton, New Jersey) as a 3-dimensional surface overlaid on the real-time MRI images (Fig. 3C).

Follow-up

After closure, animals were observed for 3 h by serial hemodynamics and MRI, with attention to pericardial and pleural fluid, and by radiocontrast angiography. Serum and pericardial hematocrit and (human) cardiac troponin I (i-STAT, Abbott, Princeton, New Jersey) were measured.

Follow-up was pre-specified for days 1 to 3 and 5 and weeks 4 and 12 and included MRI to evaluate device position, LV function, myocardial scar, and pericardial and pleural fluid volume. Euthanasia at pre-specified time points allowed necropsy samples at weeks 1, 4, and 12.

Pathology

Necropsy examination of the heart, pericardium, and muscular VSD occluder was performed in all. Histological analysis was performed 3 months after the procedure. Sections were examined by light microscopy for the presence of inflammation, thrombus, neointimal formation, and injury following toluidine blue and basic fuchsin staining.

Data analysis

Statistical analysis used GraphPad Software, La Jolla, California). Numerical parameters are reported as mean ± SD or median (interquartile range) as appropriate. Continuous repeated parameters were tested using analysis of variance, 2-tailed paired *t* test, or Wilcoxon matched-pairs signed-rank test, as appropriate, and $p < 0.05$ was considered significant.

Results

Initial feasibility of percutaneous access and closure of LV

The technique was developed in 8 animals that were sacrificed; 3 underwent only percutaneous LV access and 5 underwent both access and closure. During these experiments, 1 case of septal injury by the 18-F sheath was attributed to an excessively soft 0.035-inch guidewire that was replaced with a stiff one in later experiments. In another case, the occluder was withdrawn from the myocardial hole due to accidental retraction. Thereafter, experiments used a backup wire to prevent this complication, although it was never required thereafter.

Safe and targeted percutaneous LV access achieved with real-time MRI guidance

Eleven animals had percutaneous LV access and closures guided by real-time MRI and were kept alive up to 3 months. The use of an active needle enabled clear visualization of the device in relation to soft tissues along the needle trajectory (Fig. 2) from skin puncture to LV cavity entry. This allowed selection of an optimal puncture site for potential future aortic or mitral access while avoiding injury to papillary muscles, interventricular septum, or mitral valve structures (Figs. 3A and 3B, Online Video 1). Coregistration of coronary CT angiography assured the operator that the needle would not injure a coronary artery (Fig. 3C). Follow-up coronary angiograms verified intact coronary arteries in all.

Left ventricular puncture and sheath placement provoked isolated premature ventricular contractions but no sustained arrhythmia. Heart rate (100 ± 19 vs. 100 ± 16 beats/min, respectively) and systolic arterial blood pressure (75 ± 7 vs. 79 ± 11 mm Hg, respectively)

remained unchanged from baseline to puncture and 18-F sheath delivery (Figs. 4A and 4B). Left ventricular puncture and 18-F sheath placement caused minor pericardial hemorrhage (30 ± 26 ml).

The time required to access the LV and introduce an 18-F sheath was 29 ± 9 min. The 18-F sheath remained inside the LV for 29 ± 9 min.

Early effects of muscular VSD occluder-mediated closure of apical access site

In all animals (n = 11), the occluder device was successfully deployed inside the LV wall puncture tract. Real-time MRI depicted the distal ("endocardial") and proximal ("epicardial") disk deployment (Figs. 5A and 5B) with respect to the cardiac structures and LV free wall, enabling the operator to perform safe device deployment (Online Video 2).

During device deployment, "permissive pericardial tamponade" was temporarily induced to separate visceral and parietal pericardium by instilling 213 ± 76 ml of saline into the pericardial space under real-time MRI guidance. This technique efficiently separated the 2 pericardial layers (Figs. 5A and 5B) in 8 of 11 cases with transient 42 ± 10 mm Hg (57 ± 13%) decrease in systolic blood pressure from baseline. During the exchange of the 18-F sheath and occluder device deployment, 149 ± 246 ml of blood also accumulated in the pericardial space. Immediately following device deployment, all pericardial fluid was aspirated (total of 363 ± 283 ml) with stabilization of the systolic arterial blood pressure (73 ± 12 mm Hg) compared with baseline (79 ± 11 mm Hg) (Fig. 4B, Online Video 2). Left ventricular closure was accomplished in 15 ± 8 min.

During the 3-h post-procedure observation period, animals were hemodynamically stable (Fig. 4). X-ray ventriculography and serial MRI indicated no shift in device position or contrast extravasation (Figs. 5C and 5D).

A total of 9 ± 5 ml of fluid accumulated in the pericardial space (pericardial fluid hematocrit of 4 ± 2%) during the 3-h observation without a change in serum hematocrit (Fig. 4C). As expected during myocardial traversal, cardiac troponin I levels increased from 0 (interquartile range [IQR]: 0 to 0.04) at baseline to 0.39 (IQR: 0.2 to 0.9) ng/ml at 3 h ($p = 0.004$).

All animals had early (day 5 ± 1) pericardial fluid accumulation. Because it was not feasible to leave a post-procedure pericardial drain in these animals, a single peri-cardiocentesis was performed on day 5 ± 1 to aspirate 192 ± 118 ml of fluid (hematocrit 2%). Thereafter, no further pericardial or pleural fluid accumulated in animals with appropriately positioned devices.

Complications associated with percutaneous closure

Within the survival animal cohort (n = 11), immediately after device deployment, 2 animals had bloody right pleural effusion that was drained and did not recur.

In 3 of 11 survival animals, the pericardium was entrapped by the "epicardial" occluder disk. This "tethered" open the LV access tract, resulting in tamponade and early death in 2 and nonlethal late pericardial effusion at 1 month in the third.

A third animal died early because the selected puncture site was the true apex. In this animal, the "endocardial disk" was deformed dynamically by the contracting apical myocardium, preventing effective hemostasis of the LV access port.

Late evaluation of apical access port after percutaneous closure

Of the surviving animals (n = 8), 2 were kept alive for 1 week, 4 for 1 month, and 2 for 3 months. As represented in Figure 4D, percutaneous LV access and subsequent closure did not adversely affect LV function. Baseline LV ejection fraction (0.40 ± 0.07) did not change early (0.43 ± 0.07 at 2 days) or late (0.39 ± 0.05 at 1 month, and 0.48 ± 0.05 at 3 months) after the procedure.

No LV myocardial fibrosis developed beyond the access site as evaluated by delayed gadolinium enhancement MRI studies at follow-up. No pleural effusion accumulated during the follow-up period.

Pathology

Macroscopic pathological evaluation at weeks 1, 4, and 12 indicated that the device remained inside the puncture tract (Fig. 6). No intracavitary LV thrombus was found.

The epicardial disk was deployed appropriately inside the pericardial space in 12 of 15 animals. In 3 animals from the survival cohort, the epicardial disk entrapped the parietal pericardium.

Histology examination at 3 months showed that both occluder disks were well opposed to the endo- and epicardial surfaces of the ventricle. The endocardial surface was fully endothelialized with no surface thrombus formation. The epicardial retention disk was fully incorporated with well-organized smooth muscle growth, moderate angiogenesis, and moderate-to-severe inflammatory cells. All inflammatory reaction was contained within or in close proximity to the device. Overall, there was occlusive infiltration of the muscular VSD occluder with rich proteoglycan matrix, smooth muscle cells, angiogenesis, and chronic inflammatory cells.

Discussion

We describe a novel approach for percutaneous closed-chest direct transthoracic access to the beating heart using large devices intended for structural heart therapies. Real-time MRI is a powerful tool for accurately guiding the interventional procedure, by providing instantaneous display of the entire thoracic context and cardiac target to the operator.

As structural heart disease therapies become more sophisticated, direct transapical perventricular access options become more important. A large minority of patients undergoing transcatheter aortic valve replacement require transapical access because of iliofemoral arteries that are small, tortuous, calcified, or occluded (15). Transapical access is often required for percutaneous repair of paravalvular regurgitation (4) and could enable transcatheter implantation of large mitral valve prostheses (5). Percutaneous, closed-chest, direct LV access would be an attractive alternative to the current practice of open-chest, surgical transapical approach, which is associated with morbidity and prolonged hospitalization (1).

Procedural failures in the present study were primarily due to unfamiliar technique during early development and use of an occluder device purpose-built for a different application. This limitation should not detract from the important finding that large operative appliances could be introduced and removed from the heart without surgical exposure. Furthermore, 3-month follow-up of LV function and histology demonstrated the safety and durability of the device in the LV free wall.

Design implications

The double-disk occluder design appears to anchor sufficiently during deployment and during healing, and it appears to accommodate the contracting myocardium. However, the commercial muscular VSD closure device was not designed for this application. Its porosity (16) may contribute to early bleeding, its neck length is fixed, and its pliable disks distort and malappose during cardiac contraction in a true apical position. These problems are surmountable with device customization to reduce porosity (e.g., with a surface membrane [17]) and to better conform to tract geometry. We predict this approach could scale into larger devices.

Our experience suggests that pericardial entrapment by the LV closure device may result in early or late bleeding due to the cyclic discordant motion of the 2 pericardial layers, leading to continuous movement of the device inside the transmyocardial tunnel. Our technique of "permissive tamponade" failed to ensure intrapericardial deployment of the outer disk in one-fifth of cases. Enhanced sheath designs (outer balloons, expandable meshes) may help to displace the parietal pericardium from the epicardium and to improve reliability. Pericardial displacement appears neither feasible nor necessary in cases of pericardial adhesion or absence, for example, after transmural infarction or cardiac surgery, because there is no discordant pericardial motion causing device distortion or displacement (data not shown).

The early nonrecurrent accumulation of serosanguinous pericardial fluid probably represent reactive pericardial effusion to the epicardial disk. In patients, this would be managed using temporary drains, as in surgical patients.

Alternative closure considerations

Small LV access ports (<6-F) have been allowed to close spontaneously (18,19) and more recently have been closed in animals using vascular closure staples (20) and in humans using vascular embolization coils (4). These techniques are less attractive applied to larger access ports.

The current surgical standard to close left ventricular access sites is to apply 1 or more transmural pledgeted purse-string apical sutures after minithoracotomy exposure (1). Suture-based catheter devices are under development to recapitulate this approach.

Finally, device solutions must also accommodate heterogeneity of target myocardial wall thickness identified during pre-procedure imaging, including mixed transmural and nontransmural myocardial infarction and hypertrophy.

Imaging guidance

Direct percutaneous LV access and closure requires instantaneous soft tissue imaging to identify anatomic structures and bleeding complications. The present study supports the use of real-time MRI for this application. However, alternative image guidance options exist. Biplane x-ray fluoroscopy combined with intrapericardial radiocontrast might outline epicardial targets, but they do not allow trajectory planning, thereby risking injuries to mitral subvalvular or other cardiac structures (7,8), nor monitoring for tract hemorrhage. Three-dimensional ultrasound is limited by available imaging windows and context, but intracavitary 3-dimensional ultrasound continues to evolve (21).

Roadmaps, such as 3-dimensional reconstructed rotational angiograms (22) or cardiac MRI (23) overlaid on biplane x-ray fluoroscopy allow trajectory planning. We found CT-derived roadmaps helpful to ensure that needle trajectories avoided coronary arteries. However,

roadmaps risk misregistration especially from alterations in loading conditions and displaced tissue, and they do not represent “live” data during, for example, rapidly evolving complications. Jelnin et al. (24) recently reported percutaneous direct left ventricular access in post-surgical patients using CT-derived roadmaps, and closure of smaller 5–12Fr holes using similar nitinol devices.

Conclusions

We believe this experience establishes the concept that with suitable devices and suitable imaging guidance, large cardiac access ports can be introduced and sealed without surgical exposure. Custom closure devices will improve the performance and reliability of this approach.

Supplementary Material

Refer to Web version on PubMed Central for supplementary material.

Acknowledgments

This study was supported by the Division of Intramural Research, the National Heart, Lung, and Blood Institute, and National Institute of Health grants (Z01-HL005062-08, Z01-HL006039-01, Z01-HL006040-01, Z01-HL006041-01). AGA Medical supplied customized ventricular septal defect occluder devices but did not participate in the design, conduct, or analysis of the study. National Institutes of Health and Siemens have a collaborative research and development agreement. Dr. Virmani is a consultant for Abbott Vascular, Arsenal Medical, Atrium Medical Corporation, Biosensors International, GlaxoSmithKline, Medtronic AVE, Terumo, and W. L. Gore Medical. Dr. Slack is a teaching proctor for AGA Medical/St. Jude Medical.

The authors are grateful to Katherine Lucas and Joni Taylor for assistance with animal experiments and to Victor Wright for assistance with MRI scans. The authors thank Patrick Cooke, Pat Russo, John Oslund, and Kurt Amplatz of AGA Medical Corporation for providing Amplatzer muscular VSD occluder devices.

Abbreviations and Acronyms

CT	computed tomography
IQR	interquartile range
LV	left ventricle
MRI	magnetic resonance imaging
VSD	ventricular septal defect

References

1. Bleiziffer S, Piazza N, Mazzitelli D, Opitz A, Bauernschmitt R, Lange R. Apical-access-related complications associated with trans-catheter aortic valve implantation. Eur J Cardiothorac Surg. 2011; 40:469–74. [PubMed: 21242089]
2. McVeigh ER, Guttman MA, Lederman RJ, et al. Real-time interactive MRI-guided cardiac surgery: aortic valve replacement using a direct apical approach. Magn Reson Med. 2006; 56:958– 64. [PubMed: 17036300]
3. Walther T, Falk V, Kempfert J, et al. Transapical minimally invasive aortic valve implantation; the initial 50 patients. Eur J Cardiothorac Surg. 2008; 33:983– 8. [PubMed: 18294859]
4. Martinez CA, Rosen R, Cohen H, Ruiz CE. A novel method for closing the percutaneous transapical access tract using coils and gelatin matrix. J Invasive Cardiol. 2010; 22:E107–9. [PubMed: 20516515]
5. Seeburger J, Borger MA, Tschernich H, et al. Transapical beating heart mitral valve repair. Circ Cardiovasc Interv. 2010; 3:611–2. [PubMed: 21156929]

6. Grenon SM, MacDonald S, Sidhu RS, et al. Successful ventricular transapical thoracic endovascular graft deployment in a pig model. J Vasc Surg. 2008; 48:1301–5. [PubMed: 18771890]
7. Al-Attar N, Ghodbane W, Himbert D, et al. Unexpected complications of transapical aortic valve implantation. Ann Thorac Surg. 2009; 88:90– 4. [PubMed: 19559200]
8. Brown SC, Boshoff DE, Rega F, et al. Transapical left ventricular access for difficult to reach interventional targets in the left heart. Catheter Cardiovasc Interv. 2009; 74:137– 42. [PubMed: 19405156]
9. Havranek EP, Sherry PD. Left heart catheterization by direct puncture with two-dimensional echocardiographic guidance: a case report. Cathet Cardiovasc Diagn. 1995; 35:358– 61. [PubMed: 7497511]
10. Raval AN, Karmarkar PV, Guttman MA, et al. Real-time MRI guided atrial septal puncture and balloon septostomy in swine. Catheter Cardiovasc Interv. 2006; 67:637– 43. [PubMed: 16532499]
11. Nazarian S, Kolandaivelu A, Zviman MM, et al. Feasibility of real-time magnetic resonance imaging for catheter guidance in electrophysiology studies. Circulation. 2008; 118:223–9. [PubMed: 18574048]
12. Barbash IM, Saikus CE, Ratnayaka K, et al. Limitations of closing percutaneous transthoracic ventricular access ports using a commercial collagen vascular closure device. Catheter Cardiovasc Interv. 2011; 77:1079– 85. [PubMed: 21234923]
13. Raval AN, Karmarkar PV, Guttman MA, et al. Real-time magnetic resonance imaging-guided endovascular recanalization of chronic total arterial occlusion in a swine model. Circulation. 2006; 113:1101–7. [PubMed: 16490819]
14. Thanopoulos BD, Tsaousis GS, Konstadopoulou GN, Zarayelyan AG. Transcatheter closure of muscular ventricular septal defects with the Amplatzer ventricular septal defect occluder: initial clinical applications in children. J Am Coll Cardiol. 1999; 33:1395–9. [PubMed: 10193744]
15. Ewe SH, Delgado V, Ng AC, et al. Outcomes after transcatheter aortic valve implantation: transfemoral versus transapical approach. Ann Thorac Surg. 2011; 95:1244–51. [PubMed: 21420661]
16. Holzer R, Balzer D, Cao QL, Lock K, Hijazi ZM. for the Amplatzer Muscular Ventricular Septal Defect Investigators. Device closure of muscular ventricular septal defects using the Amplatzer muscular ventricular septal defect occluder: immediate and mid-term results of a U.S. registry. J Am Coll Cardiol. 2004; 43:1257– 63. [PubMed: 15063439]
17. Tozzi P, Pawelec-Wojtalic M, Bukowska D, Argitis V, von Segesser LK. Endoscopic off-pump aortic valve replacement: does the pericardial cuff improve the sutureless closure of left ventricular access? Eur J Cardiothorac Surg. 2007; 31:22–5. [PubMed: 16952457]
18. Lim DS, Ragosta M, Dent JM. Percutaneous transthoracic ventricular puncture for diagnostic and interventional catheterization. Catheter Cardiovasc Interv. 2008; 71:915– 8. [PubMed: 18383174]
19. Pitta SR, Cabalka AK, Rihal CS. Complications associated with left ventricular puncture. Catheter Cardiovasc Interv. 2010; 76:993–7. [PubMed: 20928838]
20. Murarka S, Heuser RR. A novel method of ventricular closure following transapical access. Future Cardiol. 2010; 6:881–7. [PubMed: 21142643]
21. Vegas A, Meineri M. Core review: three-dimensional transesophageal echocardiography is a major advance for intraoperative clinical management of patients undergoing cardiac surgery: a core review. Anesth Analg. 2010; 110:1548–73. [PubMed: 20435948]
22. Lauritsch G, Boese J, Wigström L, Kemeth H, Fahrig R. Towards cardiac C-arm computed tomography. IEEE Trans Med Imaging. 2006; 25:922–34. [PubMed: 16827492]
23. Kim JH, Kocaturk O, Ozturk C, et al. Mitral cerclage annuloplasty, a novel transcatheter treatment for secondary mitral valve regurgitation: initial results in swine. J Am Coll Cardiol. 2009; 54:638–51. [PubMed: 19660696]
24. Jelnin V, Dudiy Y, Einhorn BN, Kronzon I, Cohen HA, Ruiz CE. Clinical experience with percutaneous left ventricular transapical access for interventions in structural heart defects: a safe access and secure exit. J Am Coll Cardiol Intv. 2011; 4:868–74.

APPENDIX

For accompanying videos, please see the online version of this article.

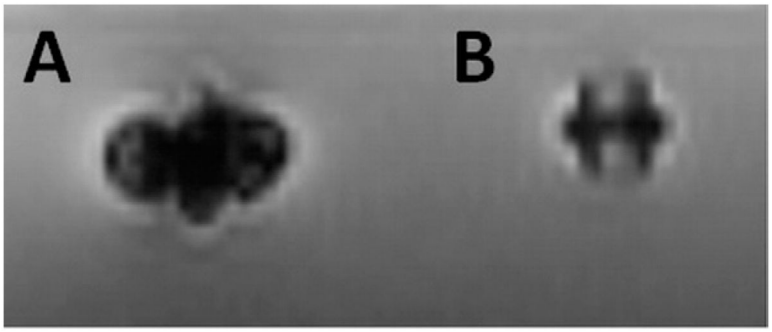

Figure 1. Ex Vivo MRI of Muscular VSD Occluder

(A) Off-the-shelf occluder with stainless steel screw creating imaging artifact. **(B)** A similar device after replacement of the device screw to a titanium screw. The device itself is made of nitinol mesh, which is passively visualized on MRI but without significant artifact. MRI = magnetic resonance imaging; VSD = ventricular septal defect.

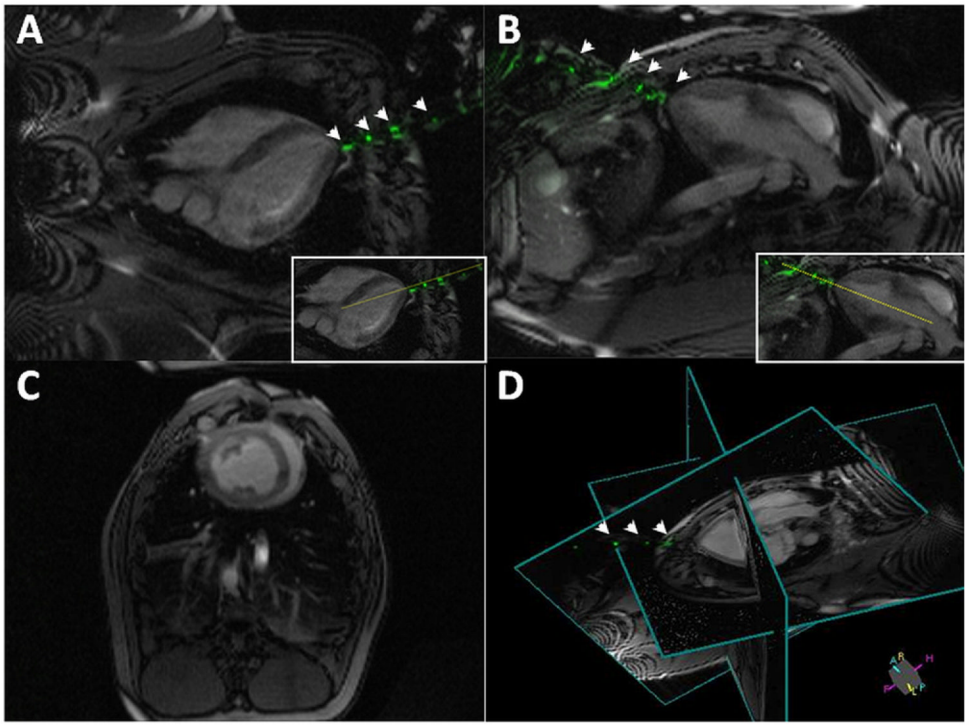

Figure 2. Real-Time MRI During LV Access

Real-time magnetic resonance imaging (MRI)-delineated 3-dimensional trajectory for the active needle by continuously updating 2 perpendicular long-axis imaging planes for needle guidance **(A,B),** 1 short-axis plane for monitoring left ventricular (LV) function **(C),** and a 3-dimensional representation of relative positioning for these 3 planes **(D).** The **dotted yellow line** in **A** and **B insets** indicate a trajectory plan for potential aortic valve intervention. This trajectory is updated continuously as the needle is advanced toward the heart. Needle markers are evident throughout the procedure **(arrowheads)**. Also see Online Video 1.

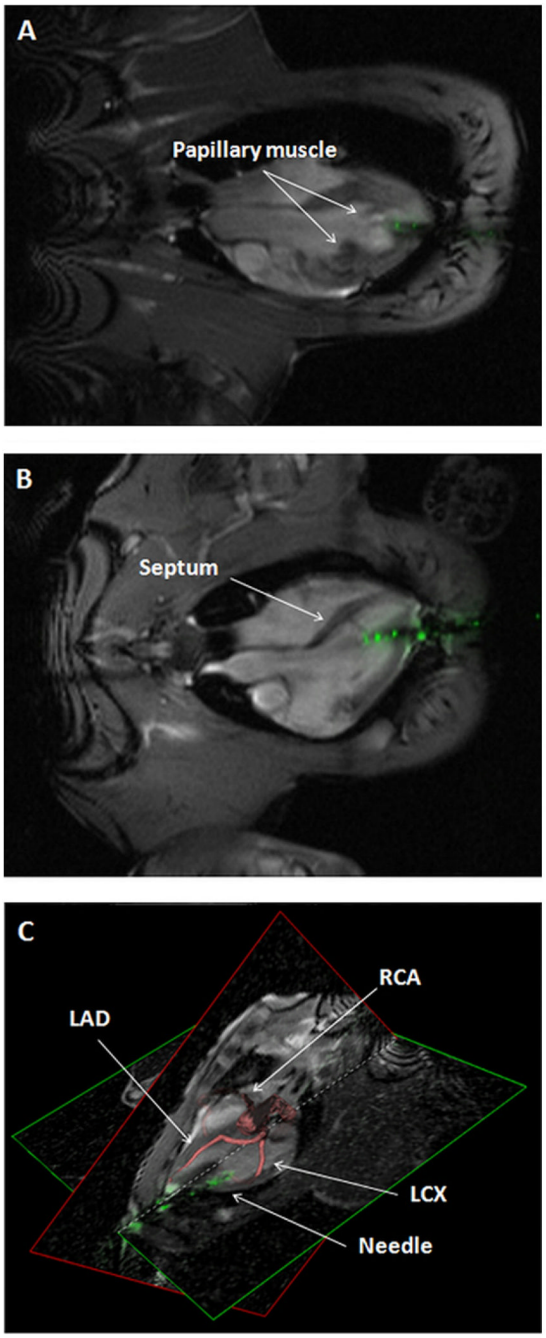

Figure 3. Cardiac Structures To Avoid During Percutaneous LV Access

Real-time procedural MRI enabled the operator to avoid injury to cardiac structures, such as **(A)** papillary muscles, **(B)** interventricular septum, and **(C)** coronary arteries. In **C,** a 3-dimensional coronary artery image (red structures) is coregistered with real-time MRI during puncture. LAD = left anterior descending; LCX = left circumflex; RCA = right coronary artery. Abbreviations as in Figures 1 and 2.

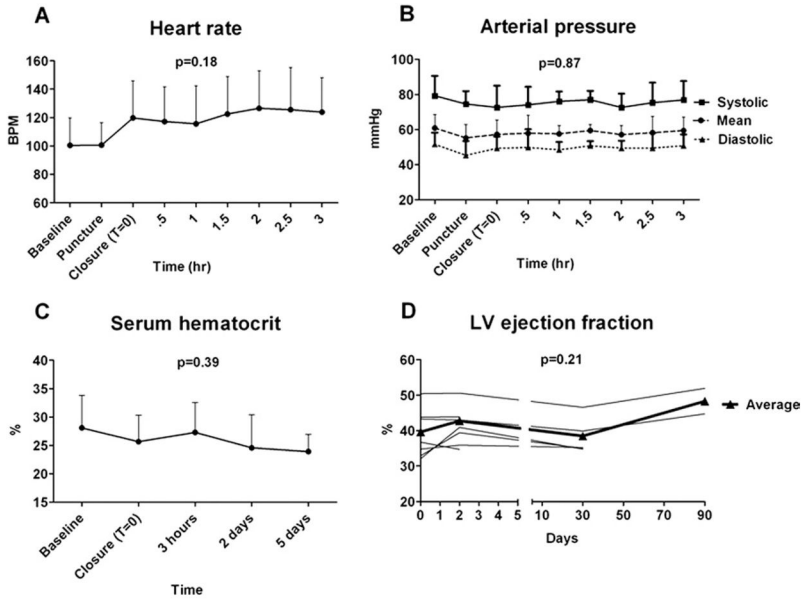

Figure 4. Hemodynamics, LV Function, and Serum Hematocrit Values During Percutaneous Direct Access and Closure of the LV

(A,B) Hemodynamics remained stable throughout the procedure. During closure of the left ventricle (LV) and following "permissive pericardial tamponade," the heart rate tended to increase **(A)** ($p = 0.18$), whereas arterial blood pressure remained unchanged **(B)** ($p = 0.87$). **(C)** Serum hematocrit remained stable during the procedure and trended downward after 5 days ($p = 0.39$ vs. baseline). **(D)** Occluder device closure had no effect on LV function early or late after the procedure. BPM = beats/min.

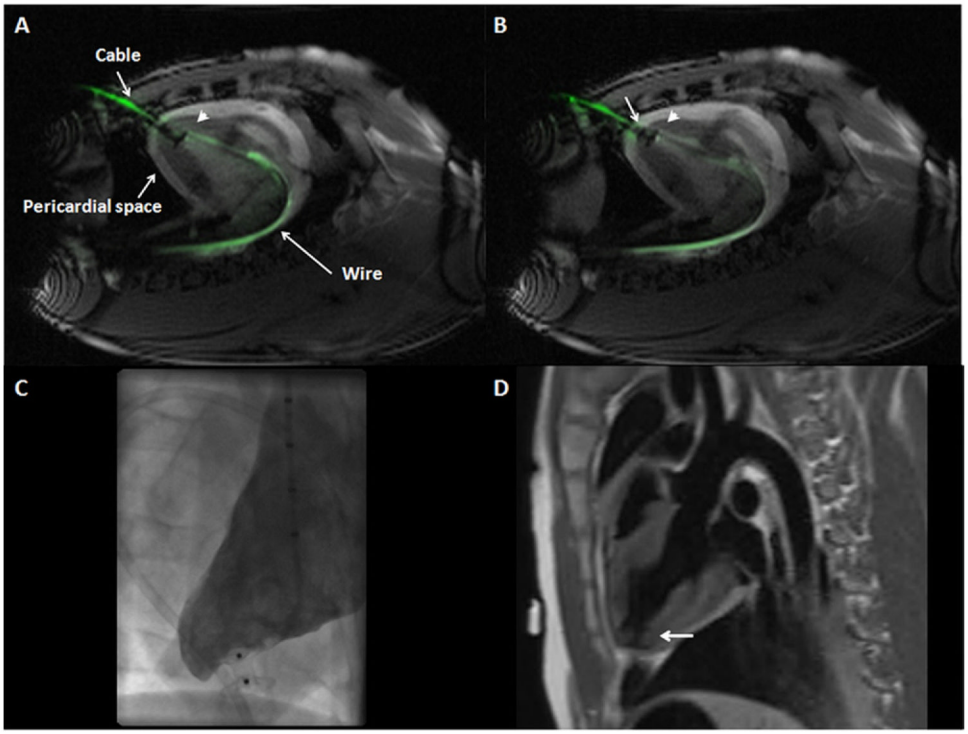

Figure 5. Muscular VSD Occluder Deployment Inside Myocardial Puncture Tract Guided by Real-Time MRI

(A,B) "Permissive pericardial tamponade" separated the parietal from the visceral pericardium by temporary instillation of fluid into the pericardial space ("pericardial space"). **(A)** The "endocardial" (distal) disk **(arrowhead)** is released inside the LV cavity in proximity to the endocardial surface. Also visible in this image is the active delivery cable ("cable") and back-up guidewire ("wire"). **(B)** The "epicardial" (proximal) disk was released against the epicardium **(arrow)** without entrapping the pericardium. Also see Online Video 2. **(C)** Early x-ray ventriculography showed occlusion of the puncture tract without extraventricular contrast leakage, and **(D)** MRI verified the correct position of the device inside the myocardial tract **(black,** indicated by the **arrow)** in a dark-blood acquisition. Abbreviations as in Figures 1 and 2.

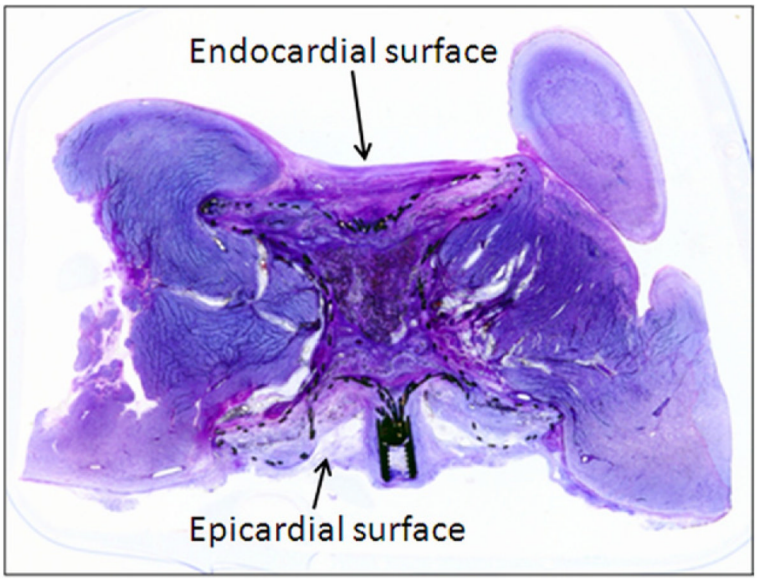

Figure 6. Pathological Evaluation of VSD Occluder Inside the LV Free Wall Myocardium

Low power image of the toluidine blue and basic fuchsin stain of the muscular VSD occluder inside the sealed myocardial access tract. Note microscopic traction of healthy myocardium over the lateral aspect of the endocardial disk by fibrosis. Abbreviations as in Figures 1 and 2.